Ultrafast Photodissociation Dynamics of Acetone at 195 nm: II. Unraveling Complex Three-Body Dissociation Dynamics by Femtosecond Time-Resolved Photofragment Translational Spectroscopy

Wei-Kan Chen and Po-Yuan Cheng*

Department of Chemistry, National Tsing Hua University, Hsinchu, Taiwan, R. O. C.

Received: February 24, 2005; In Final Form: May 12, 2005

As a continuation of the preceding paper in this issue (*J. Phys. Chem. A* **2005**, *109*, 6805), we studied photodissociation dynamics of the acetone S_2 (n, 3s) Rydberg state excited at 195 nm using femtosecond time-resolved photofragment translational spectroscopy. The technique, which is implemented by the combination of fs pump−probe ionization spectroscopy and kinetic energy resolved time-of-flight mass spectrometry (KETOF), measured temporal evolutions of the product kinetic energy distributions (KEDs) with a time resolution limited only by the laser pulse widths. Two methyl product KED components were resolved and assigned to the primary and secondary methyl products on the basis of their temporal behaviors. The results support the mechanism in which the primary dissociation occurs on the acetone S_1 surface and provide complementary dynamical information to that discussed in the preceding paper.

1. Introduction

Measurements of product energy distributions in the rotational, vibrational, and translational degrees of freedom are the most universal approaches used in studying photodissociation dynamics.[1] Through applications of various momentum and energy conservation laws, detailed dynamics, including those occurring in the transition-state region, can be indirectly retrieved or inferred in favorable cases from the measurements made long after the reaction ceases.[2,3] Among all available techniques, photofragment translational spectroscopy (PTS) is probably the most general and versatile one.[2,4,5] Although there have been many recent developments, such as the velocity map ion imaging[6,7] and H-atom Rydberg tagging,[8] all conventional PTS techniques basically measure time-integrated kinetic energy distributions (KEDs), $P(E_k)$, of fragments produced throughout the entire course of the reaction. The integrations in these conventional PTS techniques are usually from the initiation of reactions to long after they complete. Although dynamical details can be recovered from the KEDs on the basis of various conservation laws, temporal information exposed at various stages of the reaction is scrambled. For complex photodissociation reactions involving multiple pathways and/or products, momentum correlations and energy partitioning among fragments may become much more complex than those in simple two-body dissociations.[9] The situation is worsened if KEDs of different fragments overlap severely. In such cases, it is advantageous to measure the time-resolved KEDs, $P(E_k, t)$, that is, the integrated KED from the initiation of reaction to a short time t before the reaction stops. Because many elementary steps in photodissociation occur in ultrafast time scales, the temporal resolution required to measure informative $P(E_k, t)$ should be in the femtosecond (fs) to picosecond (ps) region. The additional temporal information thus obtained is particularly useful in unraveling complex photodissociation reactions involving multiple pathways and fragments of the same chemical identity.

Zewail's group has pioneered the fulfillment of this concept of fs time-resolved PTS (fs TR-PTS) by using the combination of fs pump−probe ionization spectroscopy and kinetic energy resolved time-of-flight mass spectrometry (KETOF).[10,11] They have employed resonance-enhanced multiphoton ionization (REMPI) to probe free iodine atoms produced in various types of photoreactions.[10,11] A few groups had followed this line and used ion imaging techniques to measure KEDs with fs nonresonant MPI detection.[12−14] In this work, we extent the fs KETOF technique to the detection of a polyatomic product, namely, the methyl radical, using a 2 + 1 REMPI detection scheme.[15] The results are a series of "snapshots" of product KEDs with a shutter speed of ∼200 fs. As a continuation of the preceding paper,[16] we applied this technique to elucidate the complex dynamics in the three-body photodissociation of acetone S_2 (n, 3s) Rydberg state excited at 195 nm.

In the preceding paper, we have described the use of fs pump−probe mass-selected ionization spectroscopy to measure the temporal evolutions of the initial state, intermediates, and methyl products in the photodissociation of acetone at 195 nm.[16] The results have been used to differentiate between two previously proposed mechanisms: the S_1D and T_1D mechanisms.[16] In the former case, the primary dissociation takes place on the S_1 surface,[17,18] whereas in the latter case, the primary dissociation occurs on the T_1 surface.[19−24] The mass-selected transients discussed in the preceding paper have provided some support to the S_1D mechanism and revealed a very complex dynamics involved in the reaction.[16] In addition to the temporal behaviors of the intermediates and products, measurements of the kinetic energy release are also valuable in understanding the reaction mechanisms. For the S_1D mechanism, one would expect a low kinetic energy release for the primary dissociation, because the available energy is low and there is no significant exit barrier.[17,18,25] On the other hand, the primary dissociation in the T_1D mechanism is expected to release substantial kinetic energy, because the available energy is higher and there is a significant exit barrier on the T_1 surface along the α-CC

* Corresponding author. E-mail: pycheng@mx.nthu.edu.tw.

10.1021/jp0509717 CCC: $30.25
Published on Web 07/14/2005

dissociation coordinate.[21,26] Such distinctions may be useful if the KEDs of the primary and secondary methyl products can be resolved. Unfortunately, conventional PTS studies have shown that the KEDs of the two components overlap severely.[20,21] In this work, we employed the fs TR-PTS to separate the two components on the basis of their temporal behaviors. The results again favored the S_1D mechanism and provided complementary dynamical information to that discussed in the preceding paper.[16]

2. Experimental Section

The technique of fs KETOF has been described in detail elsewhere;[10,11] therefore, only a brief description relevant to the present work is given here. The KETOF technique is basically the mass spectrometric version of the Doppler photofragment spectroscopy implemented by laser-induced fluorescence (LIF).[27−30] In general, a pump-laser pulse initiates a molecular dissociation process in the extraction region of a TOF mass spectrometer (MS). The recoiling photofragments are then ionized by a probe-laser pulse, and the resulting ions are accelerated into a field-free flight tube and detected by an ion detector. Several variants of the technique have been demonstrated over the years.[20,27−30,35−37] We chose to measure the ion TOF distribution under the space-focusing condition because of the simple relationship between the flight time and v_z. The arrival times of the ionized fragments are dispersed by the "turn-around time" $\Delta t = 2m|v_z|/qE$, where m and q are the mass and charge of the ionized fragments, E is the extraction electric field strength, and v_z is the projection of the recoil velocity along the TOF-MS axis ($\hat{z}$). Because the turn-around time is linearly proportional to $|v_z|$, the recoil velocity distribution of fragments causes a spread in the arrival time around the $v_z = 0$ fragments. The observed ion arrival time distribution, or the KETOF spectrum, is therefore a one-dimensional projection of the three-dimensional recoil velocity distribution onto the TOF-MS axis. For molecular dissociation induced by one-photon excitation of linearly polarized light, the projection of the fragment recoil velocity distribution onto the TOF-MS axis ($\hat{z}$) can be expressed as[27,31−33]

$$f(v_z, \chi) = \int_{|v_z|}^{\infty} \frac{g(v)}{2v}\left[1 + \beta P_2(\cos\chi) P_2\left(\frac{v_z}{v}\right)\right] \mathrm{d}v \qquad (1)$$

where $g(v)$ is the center-of-mass (COM) speed distribution of the fragament, χ is the angle between the photolysis laser polarization and the TOF-MS axis ($\hat{z}$), $P_2(x)$ is the second Legendre polynimial, and β is the anisotropy parameter ($-1 \le \beta \le 2$). The observed KETOF distribution is the convolution of $f(v_z, \chi)$ with some instrumental response functions. An important simplification occurs when the KETOF distribution is measured at $\chi = 54.7°$, or the "magic angle." At this angle, $P_2(\cos\chi) = 0$, and therefore, the distribution is independent of β , that is

$$f(v_z, 54.7°) = \int_{|v_z|}^{\infty} \frac{g(v)}{2v} \mathrm{d}v \qquad (2)$$

The speed distribution $g(v)$ can be obtained by differentiation

$$g(v) = -2v \frac{\mathrm{d}}{\mathrm{d}v_z} f(v, 54.7°)|_{v_z = v} \qquad (3)$$

In the fs KETOF experiments,[10,11] fs lasers are used for both the pump and the probe with a well-controlled time delay. Thus, the temporal evolution of the KETOF distributions can be measured with a time resolution limited only by the laser pulse widths.

The experimental conditions and setups, including the fs laser system, molecular beam TOF-MS apparatus, and optical arrangements, are nearly the same as those described in the preceding paper.[16] All experimental results presented in this work were obtained with a 195 nm pump and a 335.5 nm probe, unless otherwise specified. The pump laser was generated through a fs harmonic generator and excited acetone to the zero-point region of the S_2 state. The probe laser detected the free methyl radicals by using 2 + 1 REMPI via the 3p $^2A_2'' \leftarrow$ 2p $^2A_2''$ 0_0^0 transition.[15] Note that the ~2.5 nm bandwidth of the probe laser covers the entire rotational contour of the 0_0^0 band of nascent methyl products.[20] For the fs KETOF experiments presented in this work, the TOF-MS was operated under near space focusing condition with a low extraction field strength of about 100 V/cm to disperse the kinetic energy. To ensure all ions are detected, a 40-mm-diameter microchannel plate (MCP, Burle TOF-4000) assembly and a relatively short flight tube of about 55 cm were used. Both the pump- and probe-laser polarizations were oriented at 54.7° with respect to the TOF-MS axis on opposite sides.

In the "snapshot" mode, the translation stage was fixed at a specific pump−probe delay time, and then, the corresponding KETOF spectrum (i.e., the ion arrival time distribution) of the methyl products was recorded. A digital storage oscilloscope (LeCroy LT372, 500 MHz) was use to record the spectra with a sampling rate of 4 Gs/s (0.25 ns/pt). A computer program was used to automate the data acquisition. The program stops the translation stage at several preselected positions and records the KETOF spectra by averaging the ion TOF distributions for a certain number of laser shots. Background spectra due to one-laser ionization of the pump and probe alone, although very small relative to the time-dependent signal, were prerecorded by blocking one laser at a time with computer-controlled shutters at the beginning of each scan and are subtracted from the subsequently recorded pump + probe spectra. The final KETOF spectra were obtained by averaging all spectra taken at the same delay times. To avoid long-term signal drift, the program scans through these preselected positions repetitively until satisfactory spectra are accumulated. Typically, a total of 100 000 shots of signal were averaged for each KETOF spectrum presented here.

The KETOF spectra were transformed into v_z distributions using a calibration factor obtained from CH_3 speed distributions measured for the photodissociation of CH_3I at 266 nm. Because the COM of the dissociating molecule is traveling along the molecular beam axis with $v_z = 0$, the v_z distributions in the laboratory frame thus obtained are equivalent to the v_z distributions in the parent COM frame, regardless of their origins. This kinematic property arising from the experimental geometry greatly simplifies the data analyses. Because the KETOF spectra were slightly asymmetric, only the first half of each spectrum was used for analyses. The raw data were smoothed by a Savitzky−Golay numerical filter to remove high-frequency noise before they were transformed into speed distributions according to eq 3. The smoothing is necessary, because the differentiation step significantly amplifies the noise. The resultant speed distribution was transformed into KED of fragments in the precursor COM frame by $E_k = (1/2)mv^2$ and $P(E_k) = g(v)/mv$. Because the kinematics involved in three-body dissociations is complex, total kinetic energy release can be evaluated only if the primary and secondary components are clearly resolved.

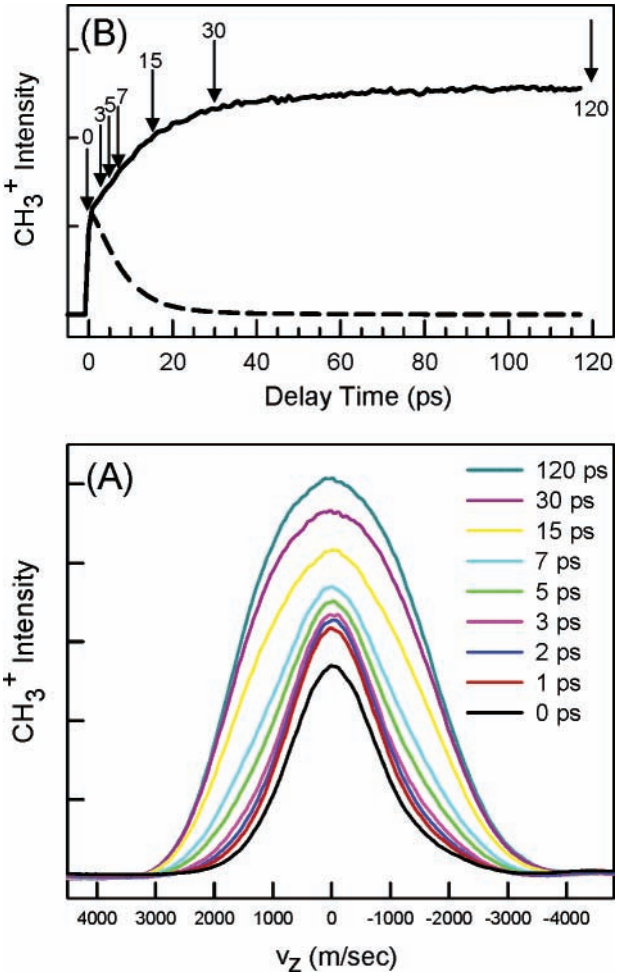

Figure 1. (A) Femtosecond time-resolved KETOF profiles measured at various reaction times indicated in the figure. (B) Methyl transient (solid trace) measured under similar conditions used for recording the KETOF spectra shown in (A). The solid arrows indicate the delay times (not all) at which KETOF spectra were recorded. The dashed trace is the dissociative ionization component resolved from the fitting described in the preceding paper.[16]

The overall speed resolution under the present conditions was about 400 m/s (at ~3500 m/s) for $m/e = 15$, as estimated from the CH_3 speed distributions measured for CH_3I photodissociation at 266 nm. The speed resolution can be improved by further reducing the extraction field strength with a sacrifice in the *S*/*N* ratio. The speed resolution is mass-dependent and is better for higher-mass fragments. For example, the speed resolution was about 150 m/s for the acetyl radical (CH_3CO, $m/e = 43$), which was also measured in this work, and was about 50 m/s for the very heavy iodine atoms ($m/e = 127$).

3. Results and Analyses

3.1. Femtosecond KETOF Spectra. Figure 1 A shows the fs time-resolved KETOF spectra obtained at various reaction times between 0 and 120 ps for the acetone photodissociation at 195 nm. The corresponding delay times in the methyl transients described in the preceding paper[16] are indicated by solid arrows in Figure 1B. The KETOF profiles change slowly with the reaction time; most importantly, the widths gradually broaden as reaction time increases, indicating that higher-speed fragments are produced at later times. Beyond 120 ps, the KETOF profiles become invariant with time, consistent with the methyl transients shown in Figure 1B. The laser pulse energies used to obtain these KETOF spectra were similar to those used for recording the transients described in the preceding paper.[16] Lowering the laser pulse energy by a factor of 2 did not change the shape of the KETOF spectra, indicating that the space−charge effect was not significant in the present case. We have also measured KETOF spectra with the pump-laser polarization parallel and perpendicular to the TOF-MS axis and found that they are nearly identical even at ~1 ps, consistent with the previous conventional PTS results reported by North et al.[21] The observations of nearly isotropic fragment angular distribution at reaction times shorter than a rotational period are consistent with the (n, 3s) excitation,[34] which has a transition dipole moment lying in the molecular plane and perpendicular to the CO bond.

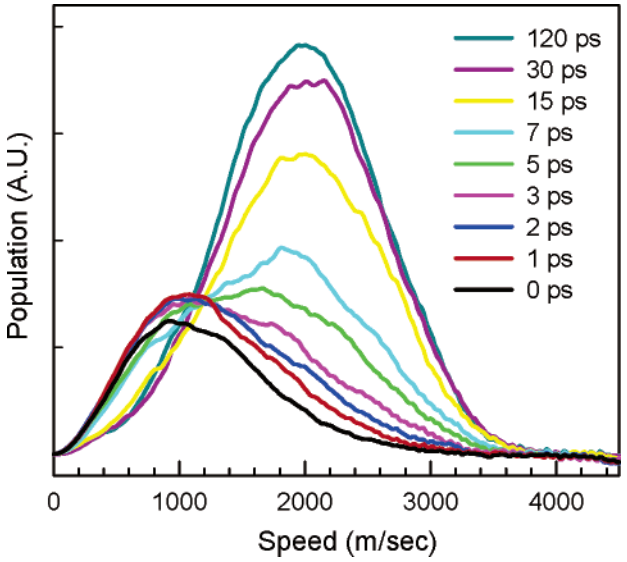

Figure 2. Femtosecond time-resolved speed distributions of CH_3^+, including those produced via ionization of neutral methyl fragments and dissociative ionization, with respect to the acetone COM at various reaction times.

Using the data analysis procedures described in the Experimental Section, we transformed each time-resolved KETOF spectra shown in Figure 1A into the corresponding speed distributions of methyl fragments shown in Figure 2. It is clear that the early-time distributions are very different from the later ones. At very early times (≤2 ps), the speed distributions appear to contain a single component that peaks at about 1000 m/s. Between 3 and 7 ps, a higher-speed component peaking at about 2000 m/s begins to grow in, and the distributions become bimodal. Beyond 7 ps, the low-speed component diminishes rapidly, but the high-speed component continues to grow until ~120 ps. The low-speed components observed at very early times were found to be nearly identical to speed distributions measured with the probe laser tuned to off-resonance wavelengths (e.g., 350 nm), suggesting that it may be due to a dissociative ionization process. Dissociative ionization is expected to release lower kinetic energy, because it usually occurs in the cationic ground state and the energy available for ion fragmentation is usually low. Moreover, the temporal behavior of the low-speed component agrees very well with the dissociative ionization component observed in the 333- and 350-nm methyl transients described in the preceding paper[16] (dashed curve in Figure 1B). On the other hand, the temporal behavior of the high-speed component is consistent with the slow-rising neutral CH_3 components observed in the 333.5 nm methyl transients.[16] We therefore assigned the low-speed component to the dissociative ionization and the high-speed component to

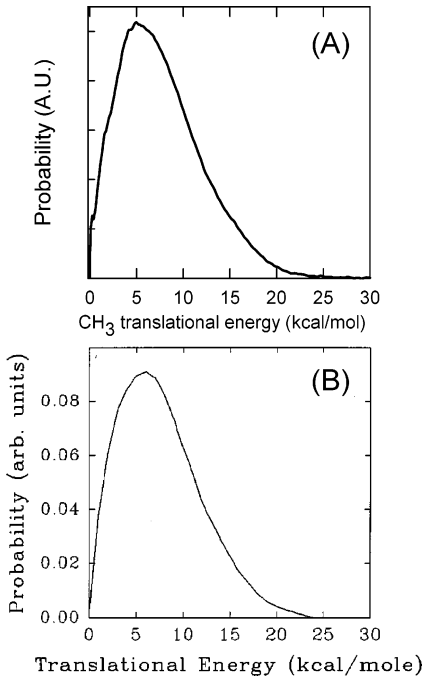

Figure 3. Comparison between (A) the kinetic energy distribution derived from our fs-KETOF spectra measured at 120 ps and (B) the kinetic energy distribution obtained by conventional long-time-integrated PTS (adapted from ref 21).

the neutral CH_3 fragments produced in the photodissociation of acetone at 195 nm.

Beyond 120 ps, the KETOF profiles become nearly invariant with time, and the dissociative ionization component decays to a negligible level. Thus, the speed distribution derived from the 120 ps KETOF spectra should be similar to those measured with conventional long-time integrated PTS. Trentelman et al. have measured the CH_3 ($v = 0$) speed distribution using a similar KETOF technique with nanosecond lasers.[20] They reported a distribution that peaks at ~2000 m/s and tails at ~4000 m/s,[20] which is quite consistent with our 120 ps speed distribution shown in Figure 2. Using conventional high-resolution PTS, North et al. reported a methyl product KED (in acetone COM frame) measured with electron-impact ionization.[21] A comparison between the methyl product KED (in acetone COM frame) derived from our KETOF spectra at 120 ps and that reported by North et al.[21] is shown in Figure 3. Evidently, the two distributions are consistent in terms of shapes and energies; though the population seems to decrease more sharply below 5 kcal/mol in our case, indicating that fewer vibrationless CH_3 products are produced with such low translational energy. The similarity between the two results seems surprising, as we are only detecting a subset of all methyl quantum states. We will discuss the implications of this similarity below.

3.2. Femtosecond KETOF of Short-Lived Acetyl Intermediate. In conventional high-resolution PTS,[4] the very long distance between the photolysis region and the detector forbids the observation of any intermediates with lifetimes much shorter than the time of flight, typically ~100 μs. Other long-time-integrated PTS techniques suffer the similar shortcoming. However, in fs TR-PTS implemented by the fs KETOF technique described here, it is possible to measure the KEDs of short-lived intermediates, provided that they can be ionized before decomposition and the ions thus produced are stable enough to survive the flight toward the detector. A very similar experiment has been reported previously using an fs ion imaging technique to measure short-lived intermediate KEDs.[12] Figure 4 shows the speed distributions derived from KETOF spectra measured for the acetyl mass channel (43 amu) at 8 and 15 ps. In this case, the transient signal at early time is dominated by dissociative ionization of the initial state, which lives for about 4 ps. Beyond ~10 ps, the dissociative ionization component is negligible, and the transient signal is dominated by the neutral acetyl fragments. Although the acetyl radical undergoes a very rapid internal conversion after the primary dissociation, it does not alter its speed and kinetic energy. These KETOF spectra and speed distributions provide important information about the primary dissociation, as the acetyl radical is the counter fragment of the primary methyl product.

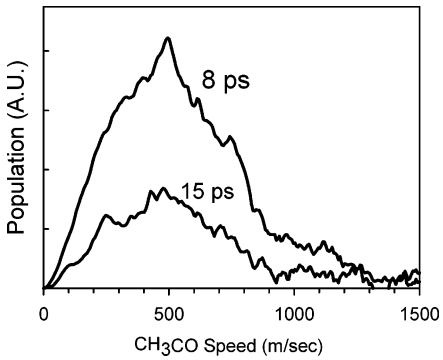

Figure 4. Speed distributions of acetyl intermediates in the acetone COM frame measured at 8 and 15 ps.

3.3. High-Kinetic-Energy Selected Methyl Transients. In addition to the "snapshot" measurements of KETOF distributions at several specific reaction times, it is also possible to "continuously" monitor the temporal behavior of methyl fragments of a selected velocity range along the TOF-MS axis. In the so-called "core-sampling"[20,35−37] configuration, different velocity regions can be selectively monitored, while the pump−probe delay time is scanned. However, in the present case, all ions are collected in order to obtain indiscriminant distributions by using a large microchannel plate (MCP) (40 mm diameter); therefore, fragments appearing in the low v_z region may contain low-speed fragments as well as high-speed ones having large recoil angles with respect to the TOF-MS axis. On the other hand, the outer region of the KETOF spectra (i.e., the high v_z region) contains high-speed fragments only. Therefore, gating the outer region of the KETOF distribution gives transients discriminated against the low-energy fragments. Figure 5B,C shows two of such transients taken by gating the ion signal within a v_z range between 1500 ± 100 and 3000 ± 100 m/s. The experimental procedures are the same as those described in the preceding paper for recording mass-selected transients,[16] except that a smaller integrator gate width corresponding to the above-specified velocity range was used to monitor the outer region of the KETOF distribution. For comparison, a methyl transient obtained by gating the entire KETOF distribution is also shown in Figure 5A. Clearly, the dissociative ionization component, which appears mostly in the low-speed region, is now greatly reduced to a minimal level. The hidden temporal feature of the neutral methyl fragments, which exhibits a characteristic of product formation in typical consecutive reactions, is now clearly revealed (see Figure 5C). The unique temporal feature of these high-KE selected transients provides valuable information on the dissociation mechanism, as discussed below.

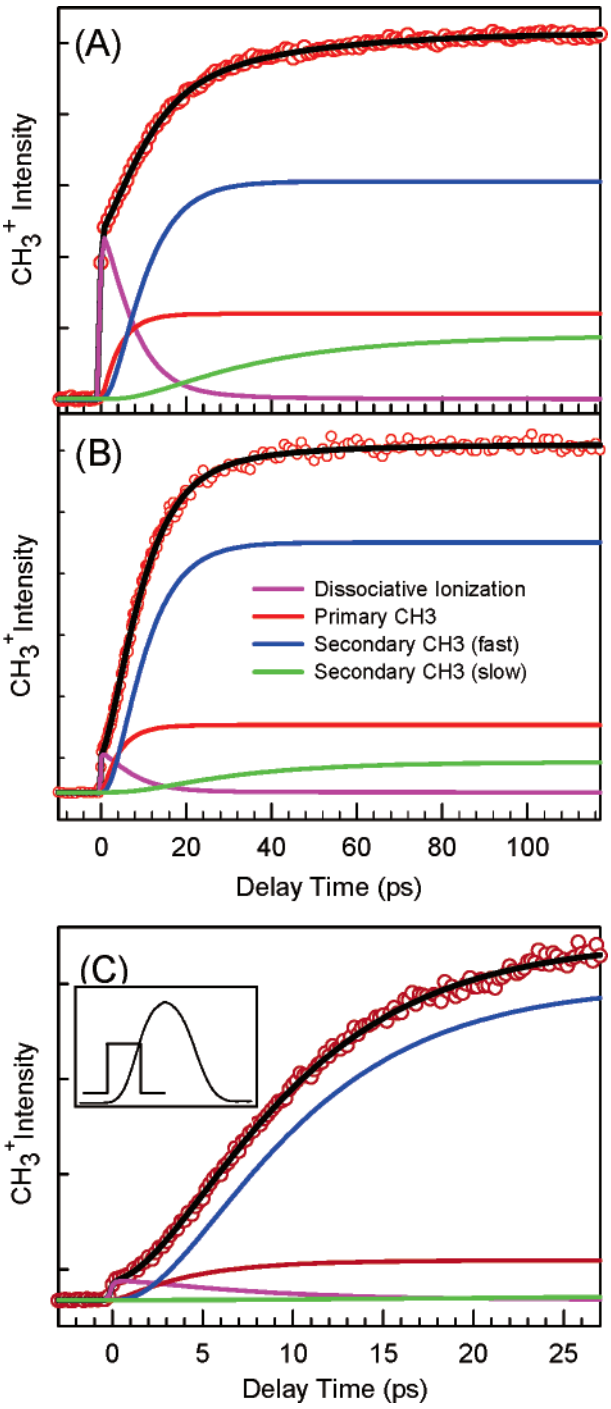

Figure 5. (A) Methyl transient measured by monitoring all methyl ions produced within the entire KETOF distribution (adapted from ref 16) (B, C) High-KE selected methyl transients measured by gating high-energy portion of the KETOF distributions. The inset in (C) schematically shows the approximate relation between the integrator gate and the KETOF profile. Note that the selected energy range was slightly higher in (C), resulting in a better energy discrimination. All fits are based on the modified S_1D kinetic model (Scheme 1) described in ref 16 with all time constants fixed at the values given therein ($\tau_1 = 4.2$ ps, $\tau_2 = 0.6$ ps, $\tau_3 = 0.1$ ps, $\tau_4 = 6.2$ ps, $\tau_5 = 25.0$ ps). The black solid lines are results of the best fits, and the colored curves are the decomposed components with their color coding indicated in (B).

4. Analyses and Discussions

In the preceding paper, we have shown that the S_1D mechanism is more consistent with the observed mass-selected transients.[16] In this section, we continue discussing the dissociation pathways and dynamics revealed by the fs time-resolved KETOF spectra and their corresponding KEDs. For the convenience of the following discussions, the energetics of relevant states and stationary points based on the best-known literature values are shown in Figure 6. The energies of acetone excited states are taken from available spectroscopic data.[26,34,38] The dissociation barrier on the acetone T_1 surface is that determined by the observation of a sudden fluorescence yield decrease.[26,39] The linear $CH_3CO(\tilde{A})$ has been predicted to lie at ~1 eV above $CH_3CO(\tilde{X})$,[17,18] whereas the barrier to α-CC dissociation on the acetone S_1 surface leading to linear $CH_3CO(\tilde{A})$ was calculated to be 77 kJ/mol (18.4 kcal/mol).[18,25] Considering the accuracy of the calculations and the acetone α-CC bond energy, these results imply that there is either a very small exit barrier or none at all on the acetone S_1 surface for α-CC dissociation. Indeed, Diau et al. have carried out complete active space self-consistent field (CASSCF) scans along the acetone S_1 α-CC minimum-energy path and found that the exit barrier is very small (<1 kcal/mol).[25] The forward barrier (71 kJ/mol) to the C−C dissociation in $CH_3CO(\tilde{X})$ is that determined by PTS studies[40] and supported by ab inito calculations.[41] As to the $CH_3CO(\tilde{X})$ exit barrier leading to CH_3 + CO, early kinetic data have suggested a value of about 25 kJ/mol.[42] However, the combination of recent PTS experiments,[41,43] thermochemical measurements,[44] and high-level ab initio calculations[41] indicated that the exit barrier in $CH_3CO(\tilde{X})$ for the C−C dissociation is between 0.36 and 0.40 eV (34.7−38.6 kJ/mol),[41,43] substantially higher than the previously reported value.[42]

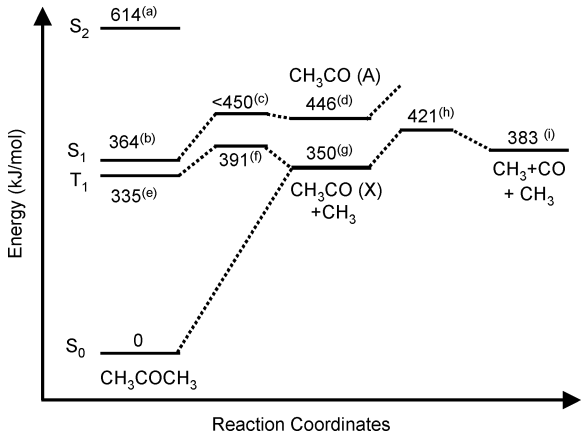

Figure 6. Energy level diagram for relevant states and stationary points involved in the photodissociation of acetone at 195 nm. All energies are in kJ/mol, include zero-point energy, and are relative to the acetone ground state. Energies were taken or derived from (a) pump-laser photon energy; (b) ref 38; (c) refs 17, 18, 25; (d) refs 17, 18; (e, f) ref 39; (g) ref 56; (h) ref 40; (i) refs 41, 43.

4.1. Femtosecond Time-Resolved Speed and Kinetic Energy Distributions: the Resolution of the Primary and Secondary Components. The traces shown in Figure 2 are, in fact, speed distributions of the methyl ions, including those produced via dissociative ionization and those produced via photoionization of the neutral methyl fragments, at various pump−probe delay times. To reveal the temporal evolution of the neutral fragment speed distributions, the contribution arising from dissociative ionization must be removed. We used the KETOF distribution taken at $t = 0$, where the signal is almost entirely dominated by dissociative ionization (see Figures 1B and 5A), as a reference and subtracted it from distributions measured at other times according to the weights of the dissociative-ionization component derived from the methyl-transient fitting described in the preceding paper (Figure 5A).[16] This procedure is justified, because ion fragmentation usually

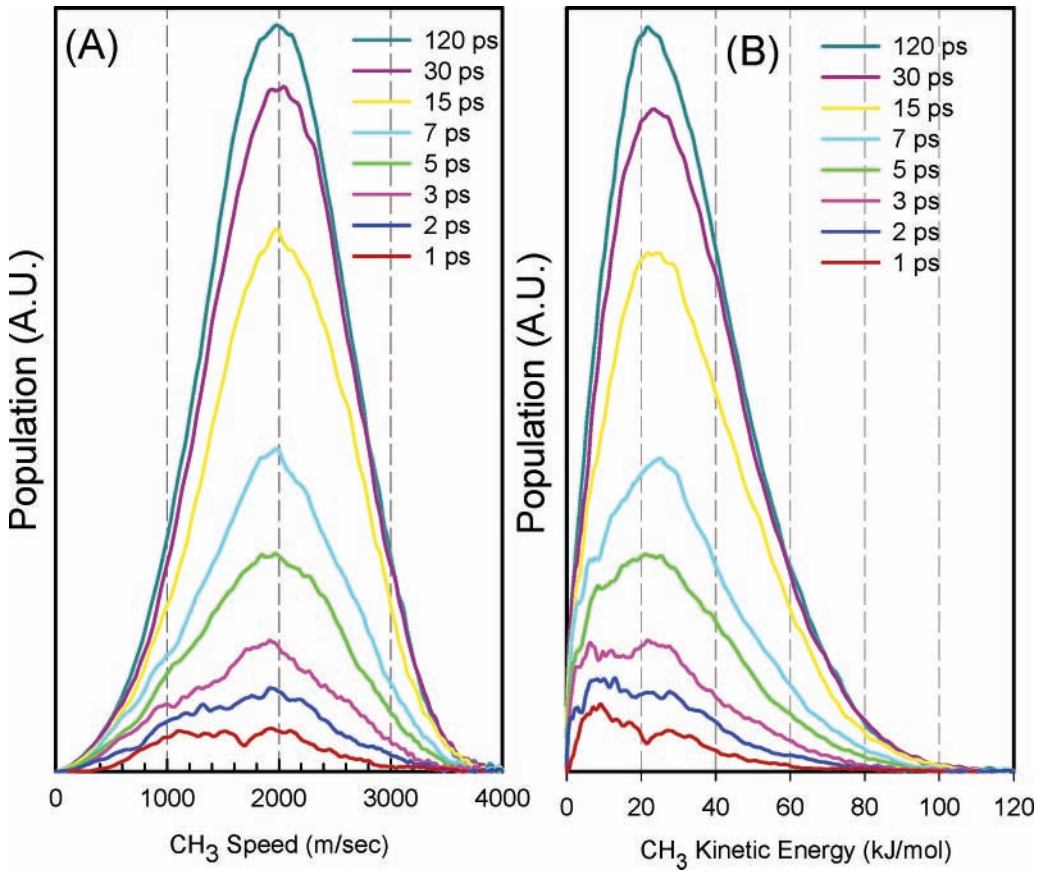

Figure 7. (A) Speed distributions of neutral methyl fragments with respect to the acetone COM obtained by removing the dissociative ionization component from the raw methyl-ion speed distributions shown in Figure 2. (B) The corresponding kinetic energy distributions of neutral methyl fragments in the acetone COM frame derived from the speed distributions shown in (A).

occurs in the cationic ground state with a time scale long enough to equilibrate the internal energy, and therefore, the methyl-ion speed distributions arising from dissociative ionization at a fixed total energy is expected to be independent of pump−probe delay time. Methyl-ion KETOF spectra measured with off-resonance probe wavelengths did show no significant variations in shapes with the delay time. Also, note that the dissociative ionization component resolved from the methyl transient is almost invariant with either mechanism (S_1D or T_1D), and therefore, any conclusions derived from these subtracted results are independent from the conclusion made in the preceding paper.[16] The results of this procedure, shown in Figure 7A, are the speed distributions of all neutral methyl fragments with respect to the acetone COM. These speed distributions are then transformed into the COM KED ($P(E_k, t)$) of neutral methyl fragments shown in Figure 7B.

These time-resolved KEDs contain detailed dynamical signatures of the reaction and provide additional supports to the S_1D mechanism. At very early times (<3 ps), the KEDs are clearly bimodal with a low-energy component peaking at ∼10 kJ/mol and a high-energy component peaking at ∼30 kJ/mol (in acetone COM frame). At 1 ps, the low-energy component is larger than the high-energy one, while at 5 ps, the two components become roughly equal. This indicates that the low-energy component rises more rapidly in the early-time region, while the high-energy component builds up more slowly. From 5 to 7 ps, the high-energy component continues to grow, but the buildup of the low-energy one slows down. Beyond 7 ps, the distributions are overwhelmed by the high-energy component and resemble the distribution observed by the conventional long-time integrated PTS[21] (see Figure 3), Because the low-energy component rises more rapidly and reaches its plateau level prior to the high-energy component, we assigned the low-energy component to the methyl fragments arising from the primary dissociation. Indeed, its temporal behavior is quite consistent with the primary methyl component resolved from the transients discussed in the preceding paper (see Figure 5A).[16] The high-energy component grows in with a much slower pace and reaches ∼90% of its plateau level at ∼30 ps, which is consistent with the secondary methyl component resolved in the methyl transient. We therefore attributed the high-energy component to the methyl fragments arising from the secondary dissociation of hot acetyl radicals. Note that we could reach these assignments on the basis of their temporal behavior alone without referring to any specific reaction pathways. The comparison with the results from the transient fittings was only meant to show the consistency between the two results.

The above assignments are in direct contradiction to the conclusions reported by North et al.[21] Although the two components overlapped severely in their methyl KEDs (see Figure 3), they have managed to resolve the two on the basis of the T_1D mechanism and the assumption that the primary distribution resembles those measured at 248 and 266 nm photolysis.[21] They concluded that the higher-energy component is due to the primary methyl and the lower-energy one is due to the secondary methyl.[21] Here, our time-resolved measurements clearly showed that it is the opposite, suggesting the invalidity of the T_1D mechanism, as it leads to an erroneous assignment.

It is also worth mentioning another seemingly possible mechanism that could give rise to the observed temporal behavior of the two components, namely, the combination of

SCHEME 1: A Kinetic Representation of the Modified S_1D Mechanism Described in Ref 16[a]

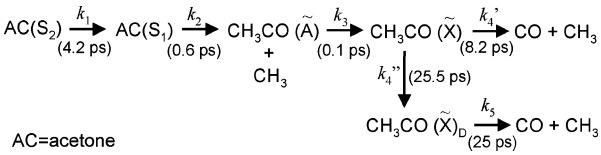

[a] The numbers in parentheses are time constants reported in ref 16.

the S_1D and T_1D mechanisms. This could occur if the $S_1 \rightarrow T_1$ ISC rate were comparable to the primary dissociation on the S_1 surface. In such a case, a fraction of the S_1 would dissociate and produce the low-energy component that appears first, and the rest will go to T_1 in which the subsequent dissociation gives the high-energy component that appears later. However, as has been discussed in the preceding paper,[16] in such a case the dissociation on the T_1 surface is expected to be much faster than that in S_1. Hence, the methyl radicals resulting from the T_1 surface, if there were any, would show an almost identical temporal behavior to those coming from S_1, not slower in time. We have also discussed the unlikelihood of the $S_1 \rightarrow T_1$ ISC being competitive with the S_1 adiabatic dissociation in the preceding paper.[16] Moreover, if the two components are both due to the primary dissociation, then it is not consistent with the near-unity three-body dissociation ($2CH_3 + CO$) yield reported by other groups.[21,47]

4.2. Further Experimental Supports. To further support the above assignments, we present the following two results as additional and independent evidence. The first is the high-kinetic-energy selected methyl transients, shown in Figure 5B,C, obtained by gating the high-energy region ($1500 \pm 100-3000 \pm 100$ m/s) of the KETOF distribution. Aside from the suppression of the dissociative ionization component, it is evident that by discriminating against the low-energy fragments the faster-rising component diminishes, while the slower-rising component still remains and dominates, indicating that those methyl fragments appearing later in time do possess higher kinetic energies. This is most evident in Figure 5C in which the selected energy range was slightly higher than that used for Figure 5B. The wavy appearance of the transient shown in Figure 5C is characteristic of the product formation in typical consecutive reactions with both steps being slow. This observation suggests that the majority of the high-KE methyl fragments are the result of secondary dissociation. The transients were fitted to the modified S_1D kinetic model described in the preceding paper with all time constants fixed at the values reported therein.[16] The modified S_1D kinetic model is shown in Scheme 1 for the convenience of following discussions. As shown in Figure 5B,C, the fits are excellent, and the results revealed that the contributions of the primary CH_3 decrease significantly in both transients, whereas the secondary CH_3 components increase and become dominant. *These results unambiguously show that the secondary dissociation does produce CH_3 fragments with higher kinetic energies in the acetone COM frame*.

The second result is the speed distributions of the short-lived acetyl intermediate shown in Figure 4. As discussed in the previous section, the KETOF distributions observed for the acetyl mass channel at 8 and 15 ps contain mostly the signal arising from ionization of neutral acetyl intermediates. The average speed of acetyl radicals derived from these two distributions at 8 and 15 ps are both about 530 m/s. On the basis of simple momentum conservation, the counter fragment (i.e., the primary methyl fragment) should possess an average speed of 1520 m/s, which is in good agreement with the average speed of the low-energy component in this time region (see Figure 7A and Table 1), and is inconsistent with the high-energy component that peaks at ~2000 m/s. *This, again, strongly indicates that the primary dissociation does produce CH_3 fragments with lower kinetic energies.*

TABLE 1: Average Speeds and Kinetic Energies Calculated Using the Deconvoluted Primary and Secondary Components Obtained in the Three-Body Kinematic Modeling

	primary component[a]			secondary component[b]		
time	$\langle v \rangle_{CH_3}$ [c]	$\langle E_k \rangle_{CH_3}$ [d]	$\langle E_k \rangle_{total}$ [e]	$\langle v \rangle_{CH_3}$ [c]	$\langle E_k \rangle_{CH_3}$ [d]	$\langle E_k \rangle_{total}$ [e]
1 ps	1400	17 ± 2	23 ± 3	2100	34 ± 3	52 ± 5
2 ps	1500	20 ± 2	27 ± 3	2150	35 ± 3	54 ± 5
3 ps	1550	21 ± 2	28 ± 3	2150	35 ± 3	54 ± 5
5 ps	1650	23 ± 2	31 ± 3	2150	35 ± 3	54 ± 5
7 ps	1650	23 ± 2	31 ± 3	2100	35 ± 3	54 ± 5
15 ps	1650	23 ± 2	31 ± 3	2100	34 ± 3	52 ± 5
30 ps	1650	23 ± 2	31 ± 3	2050	33 ± 3	51 ± 5
120 ps	1650	23 ± 2	31 ± 3	2000	32 ± 3	49 ± 5

[a] Speeds (m/sec) and kinetic energies (kJ/mol) are in the acetone COM frame. [b] Speeds (m/sec) and kinetic energies (kJ/mol) are in the acetyl COM frame. [c] Average speeds of methyl fragments; uncertanties of all speeds are ±100 m/sec. [d] Average kinetic energies of methyl fragments. [e] Average total kinetic energy releases in the primary and secondary dissociations.

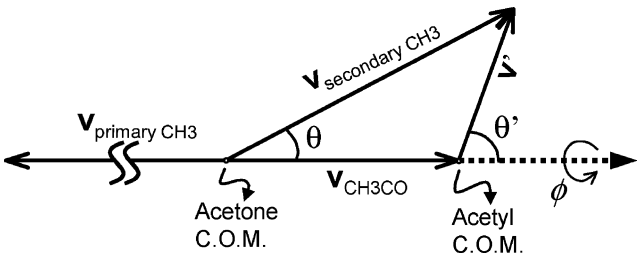

Figure 8. Vector diagram showing the relationship between fragment velocities in the acetyl and acetone COM frames used in the three-body kinematic analyses described in the text. The primed quantities are referenced to the acetyl COM and the unprimed ones to the acetone COM.

4.3. Three-Body Dissociation Kinematic Modeling. To better quantify the kinetic energy release in each step of the reaction, we have carried out three-body dissociation kinematics modeling in order to fit the observed speed distributions. The modeling procedure was similar to those described by Kroger and Riley.[48] Briefly, a primary CH_3 speed distribution function, $g(v)$, in the acetone COM frame was first assumed with some adjustable parameters, which in turn gives the corresponding speed distribution for the counter fragment (i.e., the acetyl radical). A secondary CH_3 velocity distribution function, $I'(v', \theta')$, in the acetyl COM frame was also assumed, which was then transformed into velocity distribution in the acetone frame and averaged over the acetyl speed distribution. The prime superscripts denote that the variables are referenced to the acetyl frame. The secondary CH_3 speed distribution in the acetone frame was then obtained by averaging the velocity distribution over all angles (θ'). The sum of the primary and secondary methyl speed distributions was convoluted with a Gaussian instrumental function of 400 m/s (fwhm), and the result was used to fit the experimental speed distributions using a nonlinear least-squares procedure based on the Levenberg−Marquardt method.[49] The coordinate system used in the analysis is shown in Figure 8. The primary CH_3 speed distribution was assumed to be of the form

$$g_1(v) = A_1 v^2 \exp\left[-\left(\frac{v - v_1}{\sigma_1}\right)^2\right] \quad (4)$$

where A_1, v_1, and σ_1 are adjustable parameters. The secondary methyl velocity distribution is cylindrically symmetric with respect to the primary recoil velocity and is assumed to be separable

$$I'(v',\theta') = g_2'(v')\, T(\theta') \quad (5)$$

where v' and θ' are secondary methyl speed and recoil direction in the acetyl COM frame, respectively, as defined in Figure 8. $g_2'(v')$ is the secondary CH_3 speed distribution with respect to the acetyl COM and was also assumed to have the form

$$g_2'(v') = A_2 v'^2 \exp\left[-\left(\frac{v' - v_2}{\sigma_2}\right)^2\right] \quad (6)$$

with A_2, v_2, and σ_2 being the adjustable parameters. $T'(\theta')$ gives the angular distribution of the secondary methyl with respect to the acetyl recoil direction. At delay times longer than 3 ps, an isotropic function gave excellent fits. However, at earlier times ($t < 3$ ps), an anisotropic function of $T'(\theta') = \sin^2 \theta'$ yielded better results. Although the choice of this anisotropic form is rather arbitrary, it does reflect the finite rotational motion of the acetyl fragments at early times. The fits were carried out under the constraints imposed by the primary to secondary component amplitude ratios at various times derived from the transient fitting reported in the preceding paper.[16] The fitting results were transformed into KEDs shown in Figure 9A as dashed lines, along with the experimental traces for comparison. The deconvoluted total KEDs derived from the analyses for the primary and secondary reactions in the acetone and acetyl COM frames, respectively, at various reaction times are shown in Figure 9B. The average speeds and kinetic energies of each component at different times were then calculated using the deconvoluted speed distributions and total KEDs, respectively, and are listed in Table 1.

The choices of the mathematical forms for g_1 and g_2' were rather arbitrary and only meant to extract the average kinetic energy of each component. The poor quality of the fits for the early-time (<3 ps) distributions suggested that the statistical-type functions used here may not be appropriate for the early-time dynamics, while the excellent fits for the later-time distributions suggest that a more statistical dynamics dominates in these time regions. The poor quality of the fits for the early-time distributions may also suggest the presence of a very small branching of the T_1D mechanism, which is expected to produce high-KE primary methyl fragments that appear in early time.

North et al.[21] also measured the TOF spectra of the CO product and obtained an average kinetic energy of 20 ± 2 kJ/mol in the acetone frame. Because this is a direct TOF measurement of CO without referring to any dissociation mechanism or kinematics, the value should be reliable. Although we did not measure the third product CO, it is possible to derive its KED from the primary and secondary methyl KEDs resolved in the above analyses. However, because the angular distributions of the primary and secondary dissociations are nearly isotropic, a very simple procedure can be applied to estimate the average velocity of CO by taking the vector sum of the acetyl velocity and the average CO recoil velocity in the acetyl COM frame, with the latter being perpendicular to the acetyl velocity.[20] A vector diagram for the relevant velocities is shown in Figure 10. The average speeds of the primary and secondary methyl products at 120 ps were used for this purpose. This simple procedure yielded an average speed of 1215 m/s and an approximate average kinetic energy of 20.7 kJ/mol for the CO product with respect to the acetone COM, which is in excellent agreement with the value reported by North et al.[21] This again strongly supports our assignment for the two components in the KEDs.

4.4. Time-Difference Kinetic Energy Distributions. The fs time-resolved KEDs presented so far are in fact time-integrated distributions from the initiation of reaction to a short time t defined with the ~200 fs time resolution, in contrast to the integration over a time span much longer than the reaction in the conventional PTS. It is more informative to look at KEDs of products produced within a short time interval during the reaction, i.e., the time-difference KED (TD-KED). Here, we focus on the temporal evolution of the high-energy component, i.e., the secondary dissociation. Figure 11 shows the TD-KEDs for three time intervals, 7−15 ps, 15−30 ps, and 30−120 ps. These difference spectra represent the methyl products produced within the corresponding time intervals. Because the primary methyl component reaches ~80% of its maximum level at 7 ps (see Figure 5A),[16] these TD-KEDs mainly reveal how the secondary methyl KED changes with time. As shown in Figure 11, the average kinetic energy of methyl fragments produced within these time intervals decreases with reaction time. This observation is a direct manifestation of the evaporative cooling for an isolated ensemble prepared with a broad distribution of internal energy: Those with higher internal energy within the distribution dissociate more rapidly and release higher kinetic energy, while those left behind contain less internal energy and thus dissociate more slowly and release less kinetic energy.

Close inspections of these TD-KEDs revealed additional evidence that supports our proposal of a very complex dynamics for the secondary dissociation of $CH_3CO(\tilde{X})$ due to the competition between dissociation and IVR, as described in the preceding paper.[16] The TD-KEDs for the 7−15 ps and 15−30 ps periods are similar in shape, and both center at about 30 kJ/mol, although the latter seems to shift slightly to lower energy. On the other hand, the TD-KED between 30 and 120 ps (i.e., a total of 90 ps time span) drastically shifts to a much lower energy and peaks at about 20 kJ/mol. These observations suggest that different types of dissociation dynamics dominate the two time regions and result in different product distributions. Two types of methyl fragments may be identified in the secondary dissociation: one characterized by a higher $\langle E_k \rangle$ that mainly appears between 7 and 30 ps, and the other one by a lower $\langle E_k \rangle$ that appears mostly after 30 ps with a much slower rise. According to the decomposed components obtained from the transient fitting shown in Figure 5A,[16] at 7 ps the primary methyl has risen to 80% of its maximum amplitude, and at 30 ps, the faster step (k_4') in the secondary dissociation reaches ~95% of its ultimate level. Therefore, the 7−15 ps and 15−30 ps TD-KEDs contain mostly the methyl fragments produced through the k_4' step, while the 30−120 ps TD-KED is mostly due to the k_5 step (i.e., the "dark" $CH_3CO(\tilde{X})_D$ dissociation). Because the most energetic intermediates have decomposed in the first ~6 ps, those left behind contain considerably less internal energy and thus dissociate more slowly with a time constant of 25 ps and release much lower kinetic energy. This description is also supported by the high-KE selected mass transients shown in Figure 5B,C, in which the contribution of the slower component (k_5) in the secondary dissociation also decreases, indicating that the methyl fragments produced via this step (k_5) do recoil with less kinetic energies.

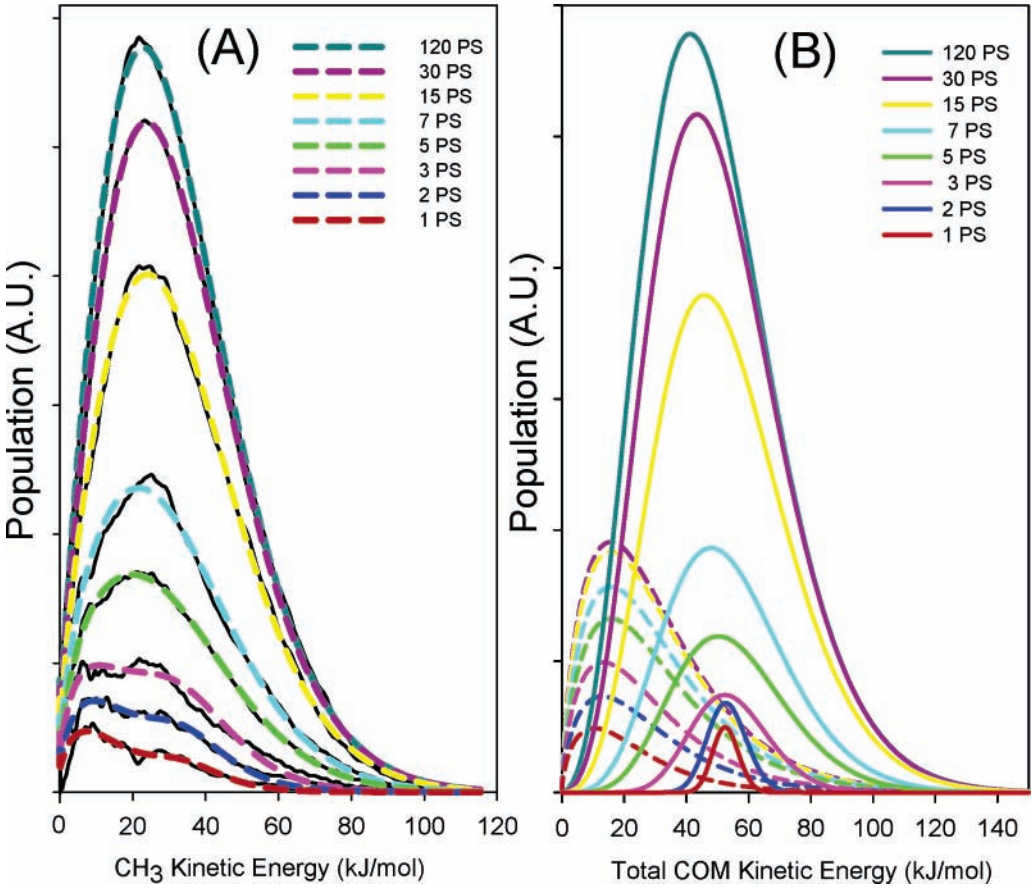

Figure 9. (A) Comparison between the CH_3 KEDs derived from the three-body kinematic modeling (dashed colored curves) and the experimental CH_3 KEDs (thin solid traces) in the acetone COM frame. (B) Deconvoluted primary (dashed lines) and secondary (solid lines) total COM KEDs obtained from the three-body kinematic fits. Note that the low-energy component at 120 ps is nearly identical to the one at 30 ps and is therefore not seen in the figure.

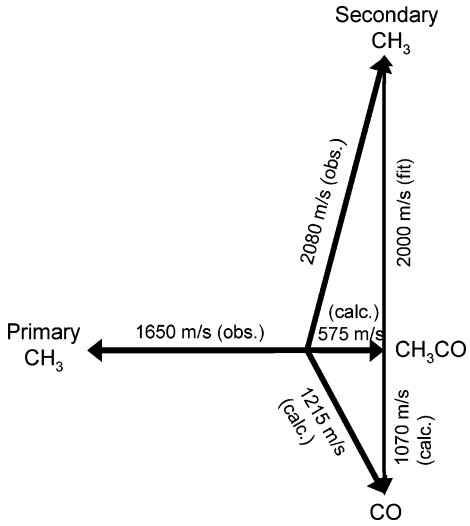

Figure 10. Newton diagram showing the relationships between the fragment average velocities in the acetone COM frame (thick arrows) and in the acetyl COM frame (thin arrows).

4.5. Primary Dissociation Dynamics. The most important result obtained in this study is that the primary and secondary methyl KED components were unambiguously resolved on the basis of their temporal behaviors. The deconvoluted primary total KED at 120 ps (Figure 9B) peaks at a low energy below 20 kJ/mol and tails at about 120 kJ/mol, which is consistent with the available energy of about 168 kJ/mol for the primary dissociation in the S_1D mechanism. On the other hand, the available energy for the primary dissociation occurring on the

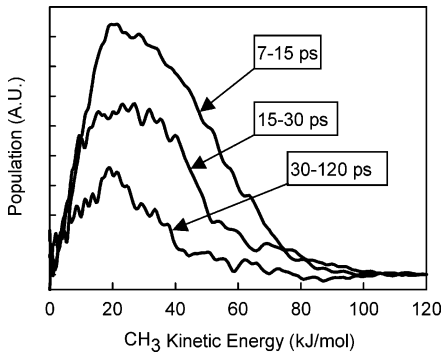

Figure 11. Time-difference KEDs obtained by taking the difference between two KEDs measured at delay times indicated in the text boxes.

acetone T_1 surface (T_1D mechanism) is 264 kJ/mol, which is less consistent with the observed primary KED unless a very large internal excitation is assumed. The deconvoluted primary total KEDs peak at low energies and give a total $\langle E_k \rangle$ of 31 kJ/mol at and beyond 5 ps, corresponding to an average fraction of available energy partitioned into the translation ($\langle f_{tr} \rangle$) of about 18%. These observations are qualitatively consistent with the primary dissociation on the acetone S_1 surface, which is characterized by a very low exit barrier[17,18,25] (<4 kJ/mol) along the α-CC cleavage coordinate.

Using a simple approach[50] based on equipartitioning of energy among all modes during the reaction, the average translational energy release in the primary dissociation can be estimated to be about 14 kJ/mol.[51] The deviation from the statistical prediction is probably not surprising if the ultrafast nature of

the primary dissociation on the S_1 surface is taken into account. This discrepancy may also suggest that the exit barrier on the acetone S_1 surface for α-CC dissociation is slightly greater than the theories predicted.[17,18,25] On the other hand, if the reaction follows the T_1D mechanism to dissociate on the acetone T_1 surface, then the much higher available energy of 264 kJ/mol and the significant exit barrier of ∼41 kJ/mol on the T_1 surface (see Figure 6) should dramatically increase the translational energy release. Indeed, North et al.[21] have estimated, using the barrier impulsive model (BIM), that the total $\langle E_k \rangle$ would be ∼60 kJ/mol for the primary dissociation occurring on the T_1 surface at 193 nm excitation. Recently, Martínez-Núñes et al.[52] carried out direct classical trajectory calculations on an acetone T_1 surface obtained from high-level ab initio calculations to predict the product energy distributions for the photodissociation of acetone at 266, 248, and 193 nm. For the 266 and 248 nm excitations, their results agreed well with the experimental KEDs reported by North et al.[21] However, at 193 nm, their results showed significant discrepancies from the experiments. The average kinetic energies for the primary and secondary methyl were found to be 49.3 and 41.0 kJ/mol,[52] respectively, which correspond to a total $\langle E_k \rangle$ of 66 kJ/mol for the primary dissociation and roughly 54 kJ/mol for the secondary dissociation in the acetyl COM frame. The former (66 kJ/mol) is consistent with the result of the BIM prediction[21] and is much higher than the primary $\langle E_k \rangle$ observed here. Notably, the classical trajectory calculations predicted that, if the reaction follows the T_1D mechanism, the primary dissociation should release more translational energy than the secondary reaction does. Thus, the theoretical considerations discussed above suggest that the primary total KED resolved here is not in accordance with the T_1D mechanism, but is qualitatively consistent with the S_1D mechanism.

The shape of the primary KED does not vary significantly with time, except that the most probable energy gradually shifts to a slightly higher value at later times, consistent with the average kinetic energies listed in Table 1. For the primary dissociation, the initially excited S_2 state and the subsequently formed hot S_1 state are produced with a well-defined energy. The combination of this initial preparation and dynamics (k_1 and k_2 in Scheme 1) may be the reason for the rather time-independent shape of the primary KEDs. This is to be compared with the secondary dissociation, in which the hot CH_3CO intermediates are produced with a broad internal energy distribution.

4.6. Secondary Dissociation Dynamics. Following the primary dissociation, the resultant $CH_3CO(\tilde{A})$ then rapidly internally converts to the ground state, $CH_3CO(\tilde{X})$, according to the S_1D mechanism described in the preceding paper.[16] The vibrational energy deposited in $CH_3CO(\tilde{X})$ comes from the vibrational excitation during the primary dissociation and the electronic−vibrational energy conversion in the ultrafast $\tilde{A} \rightarrow \tilde{X}$ IC. The former has been estimated to be about 68 kJ/mol in the preceding paper,[16] and the latter is simply the ∼96 kJ/mol energy gap between the acetyl $\tilde{A}$ and $\tilde{X}$ states.[17,18] The hot $CH_3CO(\tilde{X})$ thus contains a total average vibrational energy of ∼164 kJ/mol and readily undergoes a secondary dissociation to produce CO and secondary CH_3 via a barrier of 71 kJ/mol. On the basis of the energetics given in Figure 6, the available energy for the secondary dissociation is about 131 kJ/mol. Note that this is the average available energy resulting from a broad vibrational energy distribution in CH_3CO ($\tilde{X}$), and therefore, it is consistent with the deconvoluted total KED for the secondary dissociation that tails at about 140 kJ/mol. The deconvoluted secondary total KEDs peak at higher energies and give a total $\langle E_k \rangle$ of about 50 kJ/mol at 120 ps, corresponding to $\langle f_{tr} \rangle \approx 38\%$. The relatively high $\langle f_{tr} \rangle$ for the secondary dissociation is a manifestation of the significant exit barrier of 38 kJ/mol along the C−C dissociation coordinate in $CH_3CO(X)$.[41,43]

One of the important findings in this study is that the secondary dissociation releases more kinetic energy (50 kJ/mol in acetyl COM frame) than the primary process (31 kJ/mol). This observation is not coherent with the general picture found in most stepwise three-body dissociation, i.e., an impulsive primary dissociation producing high-kinetic-energy primary products followed by a slow secondary dissociation that releases little kinetic energy. Nevertheless, the high kinetic energy release in the secondary dissociation concluded here is consistent with several experimental and theoretical studies. The most relevant case is the one reported by Kroger and Riley[48] for acetyl iodide photodissociation at 266 nm. They found that the primary dissociation of the C−I bond in acetyl iodide produces a highly internally excited acetyl radical containing about 188 kJ/mol of energy. The very hot acetyl radicals then undergo secondary dissociation to produce $CO + CH_3$ with a broad KED peaking at $f_{tr} \approx 30\%$, or about 56 kJ/mol. In our case, the vibrational energy in the acetyl radical is about 164 kJ/mol, and we measured an average kinetic energy release of ∼50 kJ/mol with $\langle f_{tr} \rangle \approx 38\%$, which is in good agreement with their results. Mordaunt et al.[43] have recently reanalyzed the acetyl iodide data[48] along with results of two other similar measurements for acetyl chloride and acetyl bromide using the statistical adiabatic impulse (SAI) model. The model satisfactorily predicted the product energy distributions for dissociation of hot CH_3CO prepared with three different internal energies.[43] In each case, they found that about 65% of the impulsive reservoir energy (i.e., the exit barrier) is partitioned to the translational energy, whereas the remaining 35% impulsive energy goes almost entirely to rotational excitation upon dissociation of acetyl radical. Vibrational excitation of the fragments mainly comes from the statistical reservoir above the barrier.[43] Thus, the impulsive separation along the exit valley alone accounts for about 25 kJ/mol of kinetic energy. The large amount of energy in the statistical reservoir then gives rise to another 25 kJ/mol in our case.

The temporal variation of deconvoluted total KEDs for the secondary dissociation shown in Figure 9B also provide valuable information. At very early times ($t < 3$ ps), the amounts of secondary methyl fragments are insignificant, yet our analyses showed that they are produced with very narrow distributions. As time increases, the secondary KEDs broaden up rapidly. This indicates that the small fraction of the secondary methyl fragments appearing in the first 3 ps must come from a very narrow distribution of early-born high-energy acetyl radicals. As time increases, energy randomization fills up the entire phase space, and the KED becomes broader. At 5 ps, the secondary total KED peaks at about 50 kJ/mol; it then slightly shifts to lower energy and peaks at 40 kJ/mol at 120 ps. The average kinetic energies, shown in Table 1, derived from these secondary total KEDs are consistent with this behavior. Although these variations are quite small, they are reproducible and consistent with the TD-KEDs and high-KE-selected methyl transients discussed in previous sections. This temporal evolution of secondary methyl KEDs is the result of a broad internal energy distribution in hot CH_3CO intermediates and is a manifestation of the evaporative cooling effect and the complex dynamics arising from the competition between dissociation and IVR, as discussed in section 4.4.

4.7. Comparisons with Non-State-Selected KEDs. We have shown in section 3.1 that the methyl KED observed at 120 ps is very similar to that reported by North et al.[21] with non-state-selected detection implemented by electron-impact ionization. The resemblance between the two results seems surprising at first glance, since the probing scheme employed here detected only a small subset ($\nu = 0$) of the methyl ensemble. However, it can be understood as follows. As shown in the preceding paper,[16] the amplitude ratio of the primary CH_3 ($\nu = 0$) to secondary CH_3 ($\nu = 0$) is about 1:3. Therefore, the 120 ps KED observed here consists of 25% of vibrationless primary methyl and 75% of vibrationless secondary methyl, which is consistent with the components resolved in the kinematic modeling shown in Figure 9B. This ratio is a consequence of the different vibrational excitation in the primary and secondary methyl fragments. The vibrational temperature in the umbrella mode (ν_2) was estimated to be 4000 K for the primary methyl and 870 K for the secondary methyl in the preceding paper.[16] Although no information is available for other modes, the umbrella mode is probably the most excited vibration because of its low frequency (soft mode) and the very large structural change along this coordinate upon dissociation. Therefore, these temperatures should be the upper bound for the overall vibrational temperatures. Accordingly, the secondary methyl is vibrationally very cold, and a great portion of its population is in the lower vibrational levels, including the $\nu = 0$ level detected here. Hence, the $\nu = 0$ state-selected methyl KED and the all-state KED should be very similar for the secondary methyl, which constitutes 75% of the population observed here. This is probably the main reason our 120 ps methyl KED is grossly similar to that reported by North et al.[21] The remaining 25% population comes from the much more vibrationally excited primary methyl. We have shown unequivocally in this work that the primary methyl correlates to the low-energy portion of the KED, and hence, its smaller contribution is consistent with the sharper drop in population below 5 kcal/mol in our 120 ps KED (Figure 3A). Moreover, even though the primary methyl is vibrationally very hot, it is not necessary to assume the CH_3 ($\nu = 0$) detected KED to be very different from the all-state KED. The reasons are as follows: (1) As discussed earlier, the $\langle f_{tr} \rangle$ for the primary dissociation is relatively low (~18%). If this fraction is constant under the energy conservation constraint, then the average kinetic energy release for producing moderately excited primary CH_3 is not very different from that for producing vibrationally cold CH_3. For example, for primary methyl containing a rather high vibrational energy of 50 kJ/mol, the average kinetic energy release would be about 20 kJ/mol, compared to the observed 30 kJ/mol for the vibrationless methyl. This difference is probably not significant when averaged over many lower levels with higher populations and may not be observable under the present energy resolutions. The KED for the vibrationally excited CH_3 should tail at a lower energy because of energy conservation, but the low sensitivity to detect such a low population level in both techniques would probably blur this small difference. (2) Because the counter fragment may accommodate a great portion of the available energy, vibrationally cold CH_3 is not necessarily produced with higher kinetic energy. Indeed, our deconvoluted total KED for the primary dissociation producing CH_3 ($\nu = 0$) suggested a very high vibrational excitation in the counter fragment, $CH_3CO(\tilde{A})$, with an average internal energy (vib. + rot.) of ~137 kJ/mol! Of course, this is only a small subset of the $CH_3CO(\tilde{A})$ ensemble that correlates with vibrationless CH_3. Nevertheless, this result shows that the counter fragment can take up a substantial amount of available energy while keeping the kinetic energy release low, suggesting that the primary KED may be quite robust regardless of the CH_3 vibrational state selected.

Thus, the major difference between our state-selected ($\nu = 0$) KED and the all-state KED reported by North et al.[21] is the relative weight of the primary and secondary methyl components, which is evident by the sharper drop in population below 5 kcal/mol in our 120 ps KED. The similarity observed here is not unique; examples can be found in the literatures that show similar resemblances[53,54] between CH_3 ($\nu = 0$) detected KEDs and all-state detected CH_3 KEDs in shapes and energies, but not necessarily in the ratio of different CH_3 components.[55]

5. Conclusions

In this work, we have provided convincing experimental evidence to further support the validity of the S_1D mechanism for the photodissociation of acetone at 195 nm by using fs TR-PTS. Two methyl product KED components were resolved on the basis of their temporal behaviors. The low-energy component was ascribed to the primary methyl and the high-energy one to the secondary methyl. These assignments were further supported by the high-KE-selected methyl transients that reveal characteristic slow-rising kinetics consistent with the secondary product formation and by the speed distributions of the primary counter fragments (i.e., CH_3CO), which show a momentum matching that of the low-energy component. Three-body kinematic analyses of the methyl KEDs yielded average total kinetic energy releases of 31 kJ/mol for the primary dissociation and 50 kJ/mol for the secondary dissociation (in acetyl COM frame) at 120 ps.

The low kinetic energy release in the primary dissociation is consistent with the S_1D mechanism, because the available energy is low (168 kJ/mol) and there is no significant exit barrier on the acetone S_1 surface for α-CC dissociation.[17,18,25] The higher kinetic energy release in the secondary dissociation is due to the high internal energy content in the acetyl intermediate and to the existence of a significant exit barrier (~38 kJ/mol). On the other hand, the T_1D mechanism predicts a high kinetic energy release for the primary dissociation (66 kJ/mol by classical trajectory calculations;[52] 60 kJ/mol by barrier impulsive model[21]), because the available energy is high (264 kJ/mol) and there is a significant exit barrier (41 kJ/mol) on the T_1 surface for the α-CC dissociation. Moreover, the secondary dissociation in the T_1D mechanism is expected to produce a slightly lower kinetic energy (54 kJ/mol by classical trajectory calculation[52]) than the primary step, which is contradictory to our experimental observations. Thus, the present results independently support the validity of the S_1D mechanism without referring to the conclusions drawn from the mass-selected MPI transients described in the preceding paper.[16]

In addition to the elucidation of the acetone photodissociation dynamics, the present work has also demonstrated the usefulness of fs TR-PTS in unraveling very complex photodissociation reactions. In the reaction system studied here, three fragments are produced in ultrafast time scales upon photoexcitation; among them, two are of the same chemical identity (CH_3) and recoil with very similar kinetic energies. Thus, the conventional long-time-integrated PTS was hampered because of the severely overlapped KEDs and the inability to detect the metastable primary counter fragment (CH_3CO). Ultrafast time-resolved experiments were also somewhat fogged by the relatively long initial-state lifetime, which obscures the subsequent dissociation steps that are in even faster or similar time scales. The success of the present works, including those described in the preceding

paper,[16] in elucidating such a complex three-body dissociation reaction lies in the combination of the fs mass-selected MPI and fs TR-PTS to measure the temporal behaviors of the initial state, intermediates, and products with mass and kinetic energy resolution all together. Future improvements by incorporating the velocity map ion imaging should greatly enhance the energy resolution and will prove to be invaluable in studying complex photodissociation dynamics.

Acknowledgment. This work was supported by the MOE Program for Promoting Academic Excellence of Universities (89-FA04-AA) and by the National Science Council of Taiwan, R. O. C. (NSC 92-2113-M-007-052).

References and Notes

(1) *Molecular Photodissociation Dynamics*; Ashfold, M. N. R., Baggott, J. E., Eds.; Royal Society of Chemistry: London, 1987.
(2) Schinke, R. *Photodissociation Dynamics*; Cambridge University Press: Cambridge, 1993.
(3) Butler, L. J.; Neumark, D. M. *J. Phys. Chem.* **1996**, *100*, 12801, and references therein.
(4) Wodtke, A. M.; Lee, Y. T. In *Molecular Photodissociation Dynamics*; Ashfold, M. N. R., Baggott, J. E., Eds.; Royal Society of Chemistry: London, 1987.
(5) Busch, G. E.; Wilson, K. R. *J. Chem. Phys.* **1972**, *56*, 3626; **1972**, *56*, 3638.
(6) Chandler, D. W.; Houston, P. L. *J. Chem. Phys.* **1987**, *87*, 1445.
(7) Eppink, A.; Parker, D. H. *Rev. Sci. Instrum.* **1997**, *68*, 3477.
(8) Schniedler, L.; Meier, W.; Welge, K. H.; Ashfold, M. N. R.; Western, C. M. *J. Chem. Phys.* **1990**, *92*, 7027.
(9) Maul, C.; Haas, T.; Gericke, K. *J. Phys. Chem. A* **1997**, *101*, 6619.
(10) Cheng, P. Y.; Zhong, D.; Zewail, A. H. *J. Chem. Phys.* **1996**, *105*, 6216.
(11) Zhong, D.; Bernhardt, T. M.; Zewail, A. H. *J. Phys. Chem. A* **1999**, *103*, 10093.
(12) Shibata, T.; Li, H.; Katayanagi, H.; Suzuki, T. *J. Phys. Chem. A* **1998**, *102*, 3643.
(13) Samartzis, P. C.; Bakker, B. L. G.; Parker, D. H.; Kitsopoulos, T. N. *J. Phys. Chem. A* **1999**, *103*, 6106.
(14) Unny, S.; Du, Y.; Zhu, L.; Truhins, K.; Gordon, R. J.; Sugita, A.; Kawasaki, M.; Matsumi, Y.; Delmdahl, R.; Parker, D. H.; Berces, A. *J. Phys. Chem. A* **2001**, *105*, 2270.
(15) Hudgens, J. W.; DiGiuseppe, T. G.; Lin, M. C. *J. Chem. Phys.* **1983**, *79*, 571.
(16) Chen, W. K.; Ho, J. W.; Cheng, P. Y. *J. Phys. Chem. A* **2005**, *109*, 6805.
(17) Diau, E. W. G.; Kötting, C.; Sølling, T. I.; Zewail, A. H. *ChemPhysChem* **2002**, *3*, 57.
(18) Sølling, T. I.; Diau, E. W. G.; Kötting, C.; De Feyter, S.; Zewail, A. H. *ChemPhysChem* **2002**, *3*, 79.
(19) Woodbridge, E. L.; Fletcher, T. R.; Leone, S. R. *J. Phys. Chem.* **1988**, *92*, 5387.
(20) Trentelman, K. A.; Kable, S. H.; Moss, D. B.; Houston, P. L. *J. Chem. Phys.* **1989**, *91*, 7498.
(21) North, S. W.; Blank, D. A.; Gezelter, J. D.; Longfellow, C. A.; Lee, Y. T. *J. Chem. Phys.* **1995**, *102*, 4447.
(22) Zhong, Q.; Poth, L.; Castleman, A. W., Jr. *J. Chem. Phys.* **1999**, *110*, 192.
(23) Owrutsky, J. C.; Baronavsky, A. P. *J. Chem. Phys.* **1998**, *108*, 6652.
(24) Owrutsky, J. C.; Baronavsky, A. P. *J. Chem. Phys.* **1999**, *110*, 11206.
(25) Diau, E. W. G.; Kötting, C.; Zewail, A. H. *ChemPhysChem* **2001**, *2*, 273.
(26) Zuckermann, H.; Schmitz, B.; Yaas, Y. *J. Phys. Chem.* **1988**, *92*, 4835.
(27) Mons, M.; Dimicoli, I. *Chem. Phys. Lett.* **1986**, *131*, 298.
(28) Mons, M.; Dimicoli, I. *J. Chem. Phys.* **1989**, *90*, 4037.
(29) Ogorzalek Loo, R.; Hall, G. E.; Haerri, H. P.; Houston, P. L. *J. Phys. Chem.* **1988**, *92*, 5.
(30) Penn, S. M.; Hayden, C. C.; Carlson Muyskens, K. J.; Crim, F. F. *J. Chem. Phys.* **1988**, *89*, 2909.
(31) Zare, R. N. *Mol. Photochem.* **1972**, *4*, 1.
(32) Schmiedl, R.; Dugan, H.; Meier, W.; Welge, K. H. *Z. Phys. A* **1982**, *304*, 137.
(33) Vasudev, R.; Zare, R. N.; Dixon, R. N. *J. Chem. Phys.* **1984**, *80*, 4863.
(34) Gaines, G. A.; Donaldson, D. J.; Strickler, S. J.; Vaida, V. *J. Phys. Chem.* **1988**, *92*, 2762.
(35) Syage, J. A. *Chem. Phys. Lett.* **1995**, *245*, 605.
(36) Syage, J. A. *J. Chem. Phys.* **1996**, *105*, 1007.
(37) Hwang, H. J.; Griffiths, J.; El-Sayed, M. A. *Int. J. Mass Spectrom. Ion Processes* **1994**, *265*, 131.
(38) Baba, M.; Hanazaki, I.; Nagashima, U. *J. Chem. Phys.* **1985**, *82*, 3938.
(39) Zuckermann, H.; Schmitz, B.; Yaas, Y. *J. Phys. Chem.* **1989**, *93*, 4083.
(40) North, S.; Blank, D. A.; Lee, Y. T. *Chem. Phys. Lett.* **1994**, *224*, 38.
(41) Osborn, D. L.; Choi, H.; Mordaunt, D. H.; Bise, R. T.; Neumark, D. M.; Rohlfing, C. M. *J. Chem. Phys.* **1997**, *106*, 3049.
(42) Watkins, K. W.; Word, W. M. *Int. J. Chem. Kinet.* **1974**, *6*, 855.
(43) Mordaunt, D. H.; Osborn, D. L.; Neumark, D. M. *J. Chem. Phys.* **1998**, *108*, 2448.
(44) Niiranen, J. T.; Gutman, D.; Krasnoperov, L. N. *J. Phys. Chem.* **1992**, *96*, 5881.
(45) Bauschlicher, C. W., Jr. *J. Phys. Chem.* **1994**, *98*, 2564.
(46) Anand, S.; Zamari, M. M.; Menkir, G.; Lewis, R. J.; Schlegel, H. B. *J. Phys. Chem. A* **2004**, *108*, 3162.
(47) Lightfoot, P. D.; Kirwan, S. P.; Pilling, M. J. *J. Phys. Chem.* **1988**, *92*, 4938.
(48) Kroger, P. M.; Riley, S. J. *J. Chem. Phys.* **1977**, *67*, 4483.
(49) Press, W. H.; Teukolsky, S. A.; Vetterling, W. T.; Flannery, B. P. *Numerical Recipes*, 2nd ed.; Cambridge University Press: New York, 1992; p 678.
(50) Campbell, R. J.; Schlag, E. W. *J. Am. Chem. Soc.* **1967**, *89*, 5103.
(51) Two modes, the symmetric and antisymmetric C−C stretch, out of the 24 modes in acetone transform into translational motion upon primary dissociation. Hence, the simple statistical model (ref 50) predicts that on the average $^1/_{12}$ of the available energy is partitioned into translational degrees of freedom.
(52) Martínez-Núñez, E.; Fernández-Ramos, A.; Cordeiro, M. N. D. S.; Vazquez, S. A.; Aoiz, F. J.; Bañares, L. *J. Chem. Phys.* **2003**, *119*, 10618.
(53) Pino, G. A.; Torres, I.; Amaral, G. A.; Aoiz, F. J.; Banares, L. *J. Phys. Chem. A* **2004**, *108*, 8048.
(54) Blank, D. A.; North, S. W.; Stranges, D.; Suits, A. G.; Lee, Y. T. *J. Chem. Phys.* **1997**, *106*, 539.
(55) Bracker, A. S.; North, S. W.; Suits, A. G.; Lee, Y. T. *J. Chem. Phys.* **1998**, *109*, 7238.
(56) Kerr, J. A.; Patronage, M. J. *Evaluated Kinetic Data on Gas Phase Hydrogen Transfer Reaction of Methyl Radicals*; Butterworth: London, 1976; p 171.